Dopamine D2 receptor-mediated circuit from the central amygdala to the bed nucleus of the stria terminalis regulates impulsive behavior

Bokyeong Kim[a,1], Sehyoun Yoon[a,1], Ryuichi Nakajima[b,1], Hyo Jin Lee[a], Hee Jeong Lim[a], Yeon-Kyung Lee[c], June-Seek Choi[c], Bong-June Yoon[a], George J. Augustine[b,d,e], and Ja-Hyun Baik[a,2]

[a]Division of Life Sciences, School of Life Sciences and Biotechnology, Korea University, 02841 Seoul, Republic of Korea; [b]Center for Functional Connectomics, Korea Institute of Science and Technology, 02792 Seoul, Republic of Korea; [c]Department of Psychology, Korea University, 02841 Seoul, Republic of Korea; [d]Lee Kong Chian School of Medicine, Nanyang Technological University, 637553 Singapore; and [e]Institute of Molecular and Cell Biology, 138673 Singapore

Edited by Richard D. Palmiter, University of Washington, Seattle, WA, and approved September 24, 2018 (received for review July 10, 2018)

Impulsivity is closely associated with addictive disorders, and changes in the brain dopamine system have been proposed to affect impulse control in reward-related behaviors. However, the central neural pathways through which the dopamine system controls impulsive behavior are still unclear. We found that the absence of the D2 dopamine receptor (D2R) increased impulsive behavior in mice, whereas restoration of D2R expression specifically in the central amygdala (CeA) of D2R knockout mice (*Drd2*$^{-/-}$) normalized their enhanced impulsivity. Inhibitory synaptic output from D2R-expressing neurons in the CeA underlies modulation of impulsive behavior because optogenetic activation of D2R-positive inhibitory neurons that project from the CeA to the bed nucleus of the stria terminalis (BNST) attenuate such behavior. Our identification of the key contribution of D2R-expressing neurons in the CeA → BNST circuit to the control of impulsive behavior reveals a pathway that could serve as a target for approaches to the management of neuropsychiatric disorders associated with impulsivity.

dopamine receptor | impulsivity | central amygdala | neural circuit | optogenetics

Impulsive behavior—the tendency to act in premature, risky, or inappropriate ways, without consideration of the consequences—is often associated with psychiatric conditions such as drug addiction, as well as eating and personality disorders (1–4). Increasing evidence from both human and animal studies suggests the importance of dopaminergic regulation in the pathophysiology of impulsive behavior (3, 5–7). Prior human studies indicated that highly impulsive individuals are characterized by diminished midbrain dopamine (DA) D2/D3 autoreceptor availability, which leads to enhanced DA cell firing and potentiated DA release in terminal fields following exposure to novel, salient, or rewarding stimuli (7–9). Moreover, polymorphisms of the D2 DA receptor (*DRD2*) gene in humans have been linked to impulsivity in association with reward-related behavior such as substance abuse and food addiction (10–12).

In rodents, it has been reported that D2/D3 dopamine receptors (D2/D3Rs) in the nucleus accumbens (NAc) predict trait impulsivity and cocaine reinforcement (5). Furthermore, several investigations based on pharmacological manipulations of D2Rs demonstrated the control of impulsivity mediated by D2R (13, 14). However, these experiments could not clearly distinguish the effects of stimulation and inhibition of D2R and D3R. Moreover, the complex nature of impulsivity has impeded characterization of its neural correlates.

The amygdala is implicated in the control of impulsivity, with human brain-imaging studies suggesting that changes to the amygdala system and its connectivity produce higher impulsivity (15–17), possibly reflecting a neural mechanism for addictive behavior. The central nucleus of the amygdala (CeA) plays a key role in the integration of fear- and anxiety-relevant information. This nucleus also contributes to reward-related behavior (18–21), and it has been suggested that D2Rs in the CeA might modulate such behavior (22–24).

In the present study, we aimed to elucidate the role of D2Rs within the CeA in the control of impulsive behavior. Our genetic, anatomical, and optogenetic manipulations reveal that D2R, acting on CeA inhibitory projection neurons, regulates impulsivity.

Results

D2R Expression in the CeA Modulates Impulsivity. We examined impulsive behavior in wild-type (WT) and *Drd2*$^{-/-}$ mice by using a five-choice serial reaction time task (5-CSRTT) (25). *Drd2*$^{-/-}$ mice showed a significantly higher ($^{**}P < 0.01$) percentage of premature responses (Fig. 1*B*), indicative of impulsivity, as well as a higher rate of response omission (Fig. 1*B*; $^{***}P < 0.001$) and reduced accuracy (Fig. 1*B*; $^{***}P < 0.001$) compared with WT mice ($n = 7$). These data indicate that the absence of D2R increases impulsive behavior but also causes a deficit in attentional performance.

Because impulsive behavior is often associated with compulsive behavior (1, 26), we examined whether the high impulsivity of *Drd2*$^{-/-}$ mice was associated with compulsive eating behavior. Food was offered in the aversive, bright compartment of a light/dark box

Significance

Impulsivity is a tendency to act with little or no forethought or consideration of the consequences and is a major component of various psychiatric disorders. However, little is known about the brain circuits that regulate reward-related impulsivity. Our genetic manipulations reveal that dopamine D2 receptors in the central nucleus of the amygdala have a crucial role in reward-related impulsive behavior. By using optogenetics to control the neurons that possess these receptors, we have identified elements of a neural circuit that contributes to regulating impulsivity. This information should enable approaches to managing impulsivity associated with neuropsychiatric disorders such as attention-deficit/hyperactivity disorder, bipolar disorder, and addiction-related disorders.

Author contributions: G.J.A. and J.-H.B. designed research; B.K., S.Y., R.N., H. J. Lee, H. J. Lim, Y.-K.L., J.-S.C., and J.-H.B. performed research; H. J. Lee, Y.-K.L., J.-S.C., and B.-J.Y. contributed new reagents/analytic tools; B.K., S.Y., R.N., H. J. Lim, B.-J.Y., G.J.A., and J.-H.B. analyzed data; and B.K., S.Y., R.N., G.J.A., and J.-H.B. wrote the paper.

The authors declare no conflict of interest.

This article is a PNAS Direct Submission.

[1]B.K., S.Y., and R.N. contributed equally to this work.

[2]To whom correspondence should be addressed. Email: jahyunb@korea.ac.kr.

This article contains supporting information online at www.pnas.org/lookup/suppl/doi:10.1073/pnas.1811664115/-/DCSupplemental.

Published online October 22, 2018.

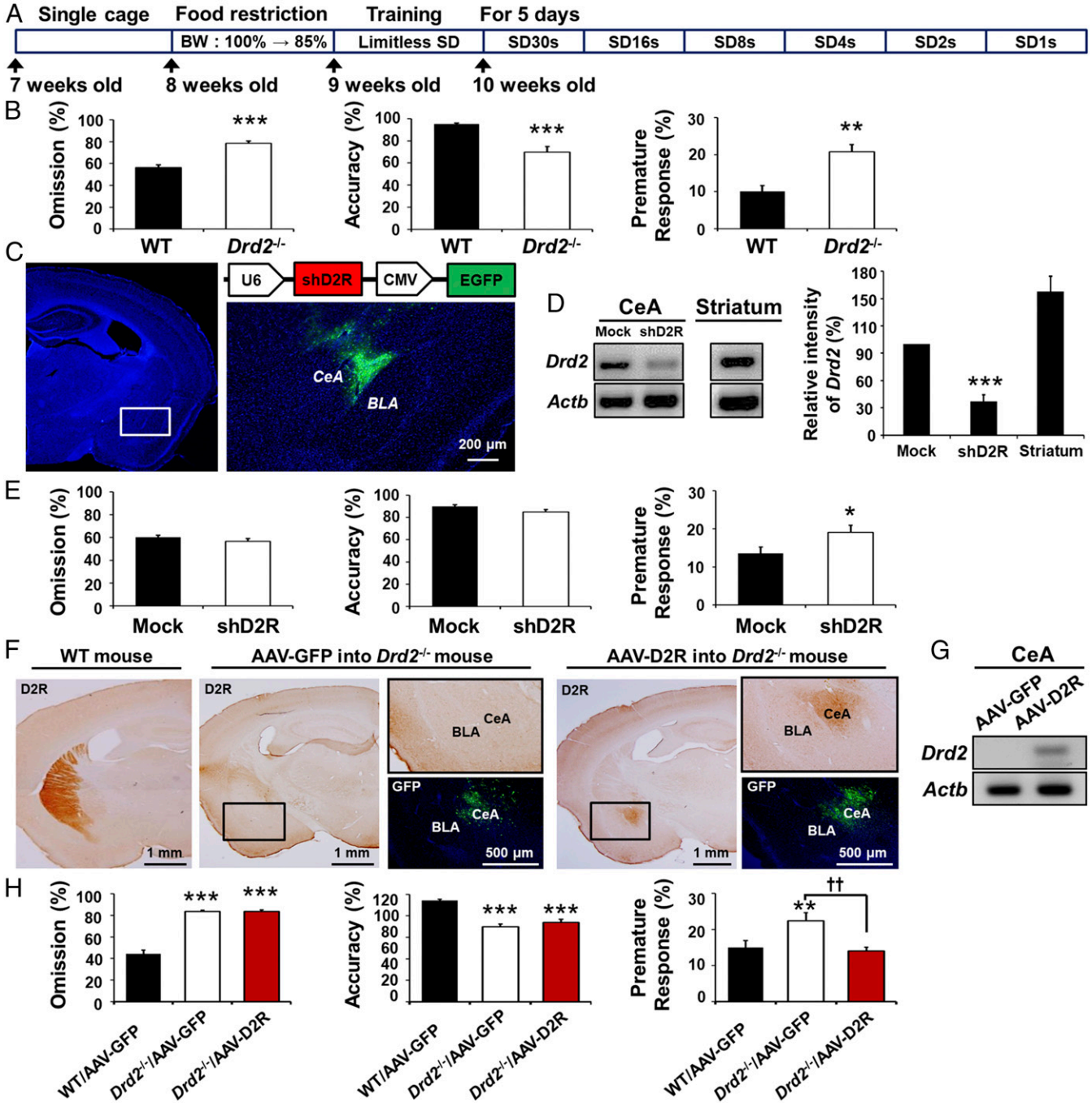

Fig. 1. D2R expression in the CeA modulates impulsivity. (*A*) Experimental scheme of the 5-CSRTT. BW, body weight; SD, stimulus duration. (*B*) Percentage omission, accuracy, and premature response, respectively, in the 5-CSRTT (ITI, 10 s; SD, 1 s) for WT ($n = 7$) and $Drd2^{-/-}$ ($n = 7$) mice. (*C*) Schematic for the lenti-shD2R vector (*Top Right*); injection site (*Left*, white rectangle) in the CeA shown in a brain section stained with 4′,6-diamidino-2-phenylindole (DAPI) (blue) and EGFP fluorescence (green) in the CeA of a mouse injected with Lenti-shD2R (*Bottom Right*, $n = 9$). U6 and CMV indicate U6 and cytomegalovirus promoters, respectively. BLA, basolateral amygdala. (Scale bars, 200 μm.) (*D*) RT-PCR analysis of *Drd2* mRNA in the CeA and dorsal striatum ($n = 6$) of WT mice injected in the CeA with lenti-shD2R ($n = 7$) or a control virus (Mock, $n = 6$) as well as densitometric quantification of the relative amount of the D2R amplicon. $^{***}P < 0.001$, One-way ANOVA. (*E*) Percentage omission, accuracy, and premature response, respectively, in the 5-CSRTT for WT mice injected in the CeA with lenti-shD2R ($n = 9$) or a control virus ($n = 9$). (*F*) Immunohistochemical analysis of D2R in the brain of a WT mouse (*Left*) or of $Drd2^{-/-}$ mice injected with AAV-GFP ($n = 8$) or AAV-D2R ($n = 8$) into the CeA (*Middle* and *Right*, respectively). [Scale bar, 1 mm (black).] [Scale bar, 500 μm (white).] (*G*) RT-PCR analysis of *Drd2* mRNA in the CeA of $Drd2^{-/-}$ mice injected as in *D*. (*H*) Percentage omission, accuracy, and premature response, respectively, in the 5-CSRTT for WT mice injected with AAV-GFP ($n = 8$) or $Drd2^{-/-}$ mice injected with AAV-GFP ($n = 8$) or AAV-D2R ($n = 8$). All values are represented as mean ± SEM; $^{*}P < 0.05$, $^{**}P < 0.01$, $^{***}P < 0.001$ versus WT with unpaired Student's *t* test (*B* and *E*) and with $^{**}P < 0.01$, $^{***}P < 0.001$ versus WT/AAV-GFP; $^{††}P < 0.01$ with one-way ANOVA followed by Bonferroni test (*H*).

(26, 27) consisting of a large white chamber (~500 lx) that was connected to a dark (~5 lx) closed chamber (*SI Appendix*, Fig. S1 *A* and *B*). After measuring initial body weight and food intake, a pretest without food was performed on WT and $Drd2^{-/-}$ mice for 15 min to determine the time spent in the light and dark chambers. Mice were then divided into two groups: one group was allowed to

eat only normal chow (NC) while the other group was given palatable food (PF) for 14 d. Mice were then returned to the light/dark box for 15 min to measure compulsive eating behavior by providing PF in the light compartment (Test, *SI Appendix*, Fig. S1 *A* and *B*). Overall, mice spent more time in the light compartment compared with their behavior during the pretest (*SI Appendix*, Fig. S1*C*). However, *Drd2*$^{-/-}$ mice consumed significantly more palatable food compared with any other group (WT NC, WT PF, and *Drd2*$^{-/-}$ NC) (*SI Appendix*, Fig. S1*D* and Movie S1; ###$P < 0.001$ versus WT, ***$P < 0.001$ versus NC, genotype × food interaction in food intake: $F_{(1,\ 77)} = 15.55$, $P = 0.0002$ with two-way ANOVA followed by Bonferroni test, $n = 21$–23). These data suggest that D2Rs are critical for regulating compulsive behavior associated with impulsivity.

To address the possible relevance of D2Rs in the CeA for control of impulsivity and anxiety, we depleted D2Rs in the CeA of WT mice by delivering a lentivirus encoding both enhanced green fluorescent protein (EGFP) and a short hairpin RNA (shRNA) specific for *Drd2* mRNA (lenti-shD2R) (28) to this brain region (Fig. 1*C*). As controls, other mice were injected with a control lentivirus. We confirmed that D2R expression in the CeA was markedly attenuated at the mRNA level in mice injected with lenti-shD2R compared with mice injected with the control lentivirus (Fig. 1*D*). Selective knockdown of D2R in CeA affected neither basal locomotor activity in the open-field test (*SI Appendix*, Fig. S2*A*) nor omission and accuracy (Fig. 1*E*) in the 5-CSRTT. However, premature responses in the 5-CSRTT were significantly increased (Fig. 1*E*; *$P < 0.05$, $n = 9$), implicating D2Rs in the CeA in the impulsivity phenotype of the *Drd2*$^{-/-}$ mice.

To further examine the role of D2Rs in CeA in impulsivity, we determined the effect of recovery of D2R expression specifically in the CeA of *Drd2*$^{-/-}$ mice. For this purpose, we injected an adeno-associated virus encoding either D2Rs and GFP (AAV-D2R) or GFP alone (AAV-GFP) as a control into the CeA of these animals (Fig. 1 *F* and *G*). This CeA-specific rescue of D2R resulted in a significant normalization of premature responses (Fig. 1*H*; ††$P < 0.01$, $n = 8$) without an effect on other parameters assessed in the 5-CSRTT (Fig. 1*H* and *SI Appendix*, Fig. S2*B*; $n = 8$). Together, these results indicate that D2Rs in the CeA regulate impulsivity.

We used D2R-EGFP mice to identify D2R-expressing neurons in the CeA, particularly in the lateral nucleus of the CeA (CeL) and the capsular nucleus of the CeA (CeC). These neurons represented about 24% of the total number of cells within the CeC and the CeL (1,918/8,071 cells). We then compared the expression of D2Rs with other proteins, such as protein kinase C-δ (PKCδ) and corticotropin-releasing factor (CRF), which are highly expressed in distinct and nonoverlapping neuronal populations within the CeL and CeC. In the CeC, PKCδ was found in 29% of D2R-expressing neurons (*SI Appendix*, Fig. S3 *A*, *C*, and *E*), and D2R was found in 33% of PKCδ cells (*SI Appendix*, Fig. S3 *A*, *C*, and *E*). In the CeL, PKCδ was in 20% of D2R-expressing neurons (*SI Appendix*, Fig. S3 *A*, *C*, and *E*), while D2R was in 36% of PKCδ cells (*SI Appendix*, Fig. S3 *A*, *C*, and *E*). In contrast, CRF was expressed mainly in the CeL, rather than in the CeC, showing weak overlap with D2R-expressing neurons in comparison with *PKCδ* (*SI Appendix*, Fig. S3 *B*, *D*, and *F*).

Photostimulation of D2R-Positive Neurons in the CeA Regulates Impulsive Behavior. To determine how D2R-expressing neurons in the CeA modulate impulsivity, we applied optogenetics to selectively stimulate these neurons. For this purpose, we injected a viral vector (AAV-DIO-ChR2-EYFP) containing a double-floxed allele for an enhanced yellow fluorescent protein (EYFP)-tagged form of channelrhodopsin 2 (ChR2) into the CeA of mice expressing a transgene encoding Cre recombinase under the control of the mouse *Drd2* gene promoter. Robust expression of ChR2-EYFP was detected in the CeA at 4 wk after virus injection (Fig. 2*A* and *SI Appendix*, Fig. S4*A*), and the fusion protein colocalized with Cre immunoreactivity in the CeA, indicating selective expression of ChR2 in D2R-expressing neurons (Fig. 2*B*). We observed that 84.8 ± 2.5% of Cre-positive neurons in the CeA also expressed ChR2-eYFP, while 89.5 ± 4.1% of ChR2-expessing neurons in the CeA were also Cre-positive (Fig. 2*B*).

Whole-cell patch-clamp recordings in brain slices were used to characterize ChR2-mediated photostimulation of CeA neurons in these virus-injected D2R-Cre transgenic mice (*SI Appendix*, Figs. S5 and S6 and Table S1). ChR2-positive (ChR2^{+}) neurons could be identified by their YFP fluorescence and by the action potentials that they generated in response to blue-light flashes (Fig. 2*C*, *Left*): 30% of CeA neurons examined (28 of 92 total cells) exhibited action potentials in response to photostimuli and another 3% of CeA ChR2^{+} neurons (3 cells) produced subthreshold depolarizations in response to light. The remaining neurons (61 cells) were ChR2-negative (ChR2^{-}) neurons that were not stimulated by light; instead, most of these (69%; 42 of the 61 cells) exhibited light-evoked inhibitory postsynaptic potentials (IPSPs; Fig. 2*C*, *Right*). To identify the source of the inhibitory inputs to these neurons, we applied laser-scanning photostimulation (29) to locally activate ChR2^{+} neurons within the CeA. Such local photostimulation evoked inhibitory postsynaptic currents (IPSCs) that were blocked by bicuculline (40 μM), indicating that they were produced by γ-aminobutyric acid (GABA)-dependent inhibitory synapses (Fig. 2*D*). Thus, photostimulation of ChR2 in D2R-expressing neurons locally inhibited neurons within the CeA.

We investigated the behavioral function of these D2R-expressing neurons in the CeA by applying optogenetic photostimulation in vivo. Bilateral photostimulation of D2R-positive neurons in the CeA (30) (Fig. 2*E*) had no effect on basal locomotor activity in the open-field test (Fig. 2*F*) or on anxiety-related behavior in the elevated-plus maze (*SI Appendix*, Fig. S4*B*). In contrast, photostimulation of these neurons resulted in a selective decrease in the proportion of premature responses without affecting omission, accuracy, or reward earning, as measured in the 5-CSRTT (Fig. 2 *G*–*I*; $n = 6$–9, interaction; $F_{(1,\ 26)} = 5.24$, $P = 0.0304$) (Movie S2). Thus, activation of D2R-positive neurons in the CeA selectively suppresses impulsive behavior.

We also examined the effect of photostimulating D2R-positive neurons expressing ChR2 in the NAc (*SI Appendix*, Fig. S7) (31). Photostimulation of D2R-expressing medium spiny neurons (D2R-MSNs) in the NAc (5-Hz, 10-ms duration light flashes) also did not affect basal locomotor activity. However, unlike photostimulation of D2R cells in the CeA, photostimulation of D2R-MSNs in the NAc increased the omission rate and simultaneously decreased the number of premature responses [*SI Appendix*, Fig. S7 *B*–*E*; $n = 6$–7, omission (%); $F_{(1,\ 22)} = 7.22$, premature response (%); $F_{(1,\ 22)} = 7.36$]. An increase in omissions is considered to be a deficit in attention, even if accuracy is unaltered. Therefore, while activation of D2R-expressing neurons in the CeA resulted in a selective decrease in impulsivity, activation of these neurons in the NAc produced both a deficit in attention and decreased impulsivity.

D2R-Expressing Neurons in the CeA Innervate the Ventral Tegmental Area and Bed Nucleus of the Stria Terminalis. We next determined the projections of the D2R-expressing neurons in the CeA that selectively control impulsive behavior. We first imaged these projections by visualizing ChR2-EYFP–expressing fibers in D2R-Cre mice with AAV-DIO-ChR2-EYFP injected into their CeA (Fig. 3*A*). EYFP-labeled axon bundles of D2R-expressing neurons in the CeA projected to the ventral tegmental area (VTA) and to the bed nucleus of the stria terminalis (BNST), as well as to other targets including the mediodorsal thalamus, basolateral amygdala, lateral hypothalamus, and substantia nigra (Fig. 3*A* and *SI Appendix*, Fig. S8 *A* and *B*). Of the projection sites identified, we focused on projections to the VTA and the BNST as candidate circuits for control of impulsivity. To reveal the specificity of this projection, we also injected a retrograde

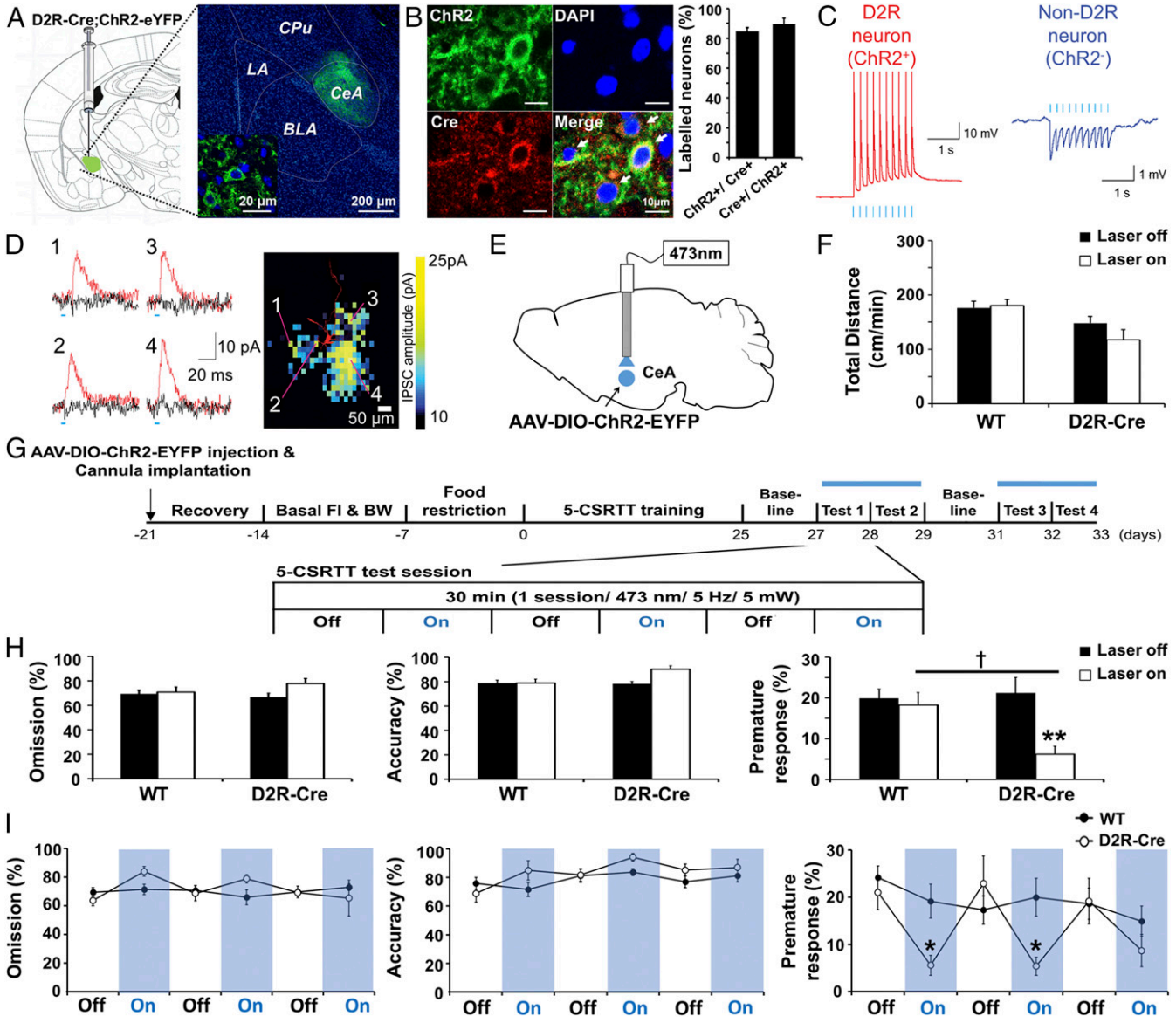

Fig. 2. Photoactivation of D2R-positive neurons in the CeA regulates impulsive behavior. (*A*) Coronal section of the brain of a D2R-Cre mouse ($n = 29$) injected into the CeA as indicated with AAV-DIO-ChR2-EYFP. The section was stained with DAPI (blue) and monitored for EYFP fluorescence (green). The CeA region is shown at higher magnification in the *Inset*. CPu, caudate putamen; LA, lateral amygdala. [Scale bars, 200 μm (main panel); 20 μm (*Inset*).] (*B*) Immunofluorescence staining for Cre as well as DAPI staining and EYFP fluorescence (ChR2) for a section of the CeA of a D2R-Cre mouse ($n = 8$) injected as in *A*. Arrows indicate a cell positive for both Cre immunoreactivity and EYFP-tagged ChR2. [Scale bar, 10 μm (*Left*).] Percentage of double-labeled cells out of the whole Cre-positive cell population and out of the whole ChR2-expressing cell population as counted from high-magnification confocal z-stacks ($n = 7$ slices per animal from two mice; total of 1,404 Cre-positive cells counted, 1,311 ChR2-expressing cells, 1,207 double-labeled cells). Quantification shows that ChR2-eYFP was expressed in 84.8 ± 2.5% of Cre-positive cells and that 89.5 ± 4.1% of ChR2-eYFP neurons were also expressed as Cre-positive signals in the CeA (*Right*). (*C*) Representative recordings of light-evoked action potentials in a ChR2-expressing D2R-positive CeA neuron (*Left*) and light-evoked IPSPs in a CeA neuron negative for both D2R and ChR2 (*Right*). (*D*) Photostimulation mapping of local inhibitory input to a ChR2-negative CeA neuron. IPSC traces were recorded with (black) or without (red) application of bicuculline (40 μM), with the numbered traces in the *Left* corresponding to the locations on the inhibitory input map on the *Right* where focal photostimulation was applied. The color scale for the map indicates the amplitude of IPSCs evoked by focal stimulation of each pixel in a voltage-clamped cell (holding potential, −50 mV). (*E*) Schematic for injection of AAV-DIO-ChR2-EYFP and implantation of a fiber-optic cannula in the CeA of D2R-Cre mice. (*F*) Total travel distance per minute in the open-field test during laser-on (3 min, 5 Hz, 5 mW) and laser-off (5 min) periods for WT ($n = 8$) and D2R-Cre ($n = 6$) mice injected in the CeA with AAV-DIO-ChR2-EYFP. The laser-off/laser-on sequence was repeated a total of four times. $P > 0.05$, genotype × light stimulation interaction; $F_{(1,\ 24)} = 1.62$ with two-way ANOVA followed by Bonferroni test. (*G*) Scheme for determining the effects of optogenetic stimulation on performance in the 5-CSRTT. Photostimulation was performed in four 30-min test sessions, each including three laser-off (5 min)/laser-on (5 min) cycles. FI, food intake; BW, body weight. (*H*) Percentage omission, accuracy, and premature response during 15 min averaged over the four test sessions of the 5-CSRTT performed with WT ($n = 9$) and D2R-Cre ($n = 6$) mice injected in the CeA with AAV-DIO-ChR2-EYFP. $^{**}P < 0.01$ versus laser off, †$P < 0.05$ versus corresponding WT value, genotype × light stimulation interaction in premature response (%); $F_{(1,\ 26)} = 5.24$, $P = 0.0304$ with two-way ANOVA followed by Bonferroni test. (*I*) Time course omission (%), accuracy (%), and premature response (%) in the 5-CSRTT as in *H*. $^{*}P < 0.05$ versus the corresponding value for WT (unpaired Student's *t* test). All data are means ± SEM.

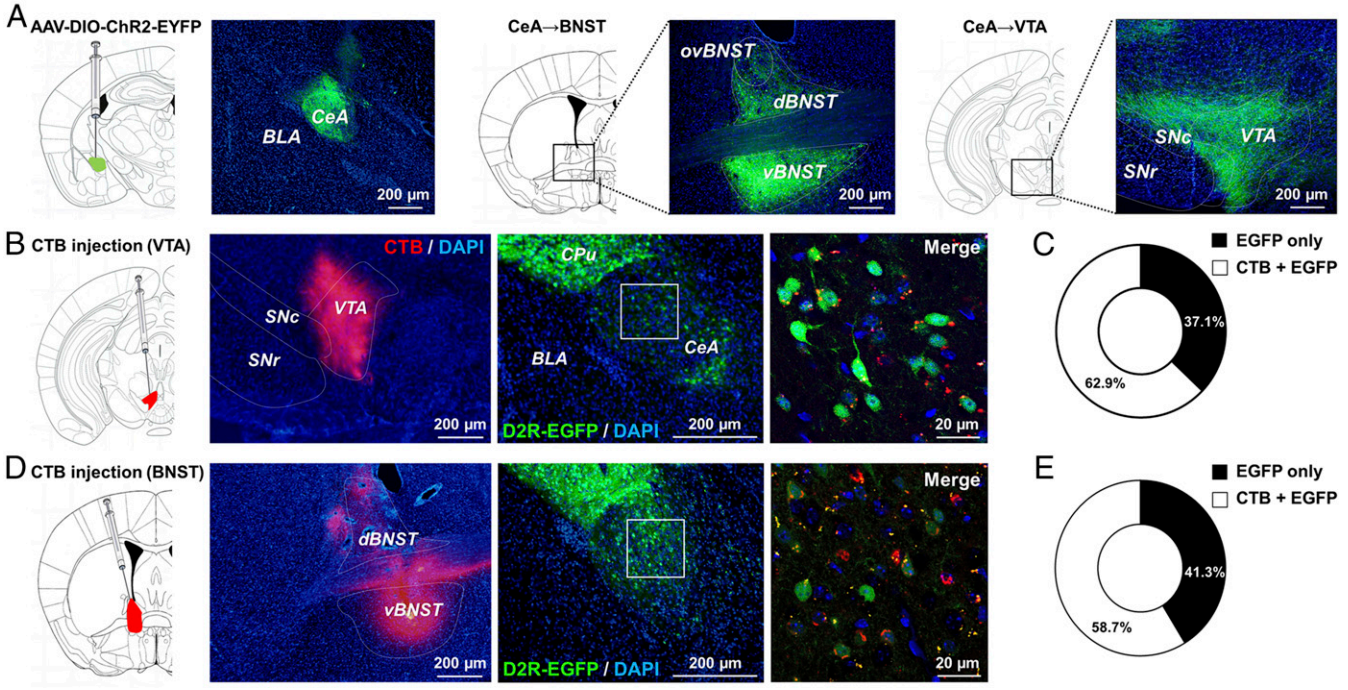

Fig. 3. D2R-expressing neurons in the CeA innervate VTA and BNST. (*A*) ChR2-EYFP fluorescence (green) in the CeA, BNST, and VTA of D2R-Cre mice ($n = 29$) injected with AAV-DIO-ChR2-EYFP into the CeA. Nuclei were stained with DAPI (blue). ovBNST, dBNST, and vBNST indicate oval, dorsal, and ventral BNST, respectively; SNc and SNr indicate substantia nigra pars compacta and substantia nigra pars reticulata, respectively. (Scale bars, 200 μm.) BNST $n = 8$, VTA $n = 13$. (*B*–*E*) Injection of the retrograde tracer CTB (labeled with Cy3) into the VTA (*B*, $n = 3$) or BNST (*D*, $n = 3$) of D2R-EGFP mice. Coronal sections of the brain show the location of the VTA (*B*) or BNST (*D*) stained with DAPI (blue) and monitored for Cy3 (CTB) fluorescence (red) in the left images and of the CeA stained with DAPI and monitored for EGFP fluorescence (green) in the central images. (Scale bars, 200 μm.) Confocal images of the CeA showing Cy3 (CTB), DAPI, and EGFP fluorescence (corresponding to the boxed regions) are shown on the *Right*. (Scale bars, 20 μm.) The corresponding proportions of EGFP-positive CeA neurons that are negative or positive for CTB are also shown. (*C* and *E*) Data were analyzed from three mice injected with CTB.

tracer—the B subunit of cholera toxin fused to a fluorescent cyanine dye (CTB)—into the VTA or BNST of mice in which EGFP expression was restricted to D2R-positive neurons within the CeA (Fig. 3 *B* and *D*). We found that 62.9% of the $EGFP^+$ neurons overlapped with CTB^+ cells when CTB was injected into the VTA and that 58.7% overlapped when CTB was injected into the BNST (Fig. 3 *C* and *E*). Similar results were obtained by injecting another retrograde tracer, DiI, into the VTA or BNST (*SI Appendix*, Fig. S9). Together, these data indicated that D2R-expressing neurons in the CeA project to both the VTA and the BNST.

To characterize the synaptic connections between the CeA and VTA, we recorded from VTA neurons in brain slices prepared from D2R-Cre mice that had AAV-DIO-ChR2-EYFP injected into their CeA (Fig. 4*A*). Photostimulation of the projections of ChR2-expressing CeA-D2R neurons evoked IPSCs in 41% of the VTA neurons examined (Fig. 4 *A* and *D*). Two types of VTA neurons can be distinguished on the basis of the absence or the presence of the hyperpolarization-activated cation current (I_h) that is found in VTA dopaminergic neurons (32). A fraction of both I_h^+ and I_h^- cells in VTA exhibited light-induced IPSCs (Fig. 4*A*). The IPSCs of I_h^- cells ($n = 20$) tended to be larger than those of I_h^+ cells (Fig. 4*B* and *SI Appendix*, Table S2; $n = 9$). However, this difference was not statistically significant ($P = 0.2$, unpaired Student's t test). Subsequent immunohistochemical staining of VTA cells for tyrosine hydroxylase (TH, $n = 24$ cells) to identify DA neurons, and of the vesicular GABA transporter (VGAT, $n = 29$ cells) to identify GABAergic neurons, revealed that half of the DA neurons sampled (6/12) received inhibitory input from the CeA (Fig. 4 *C* and *D*). GABAergic neurons represented ∼31% of VTA cells (9/29) from which we obtained recordings, and about half of these cells (5/9) also received inhibitory input from the CeA (Fig. 4 *C* and *D*). These results indicate that CeA-D2R cells send inhibitory input to both DA and GABA neurons in the VTA. Despite the presence of these inhibitory inputs of CeA-D2R neurons to the VTA, in vivo photostimulation of CeA-D2R projections within the VTA (Fig. 4*E*) had no substantial effects on locomotor activity in the open-field test (Fig. 4*F*) or on anxiety-related behavior in the elevated-plus maze (*SI Appendix*, Fig. S10*B*). Similarly, such photostimulation did not affect the proportion of premature responses or other parameters measured in the 5-CSRTT (Fig. 4 *G* and *H*; $n = 7$–13, and Movie S3). Thus, it appears that activating CeA D2R neurons does not decrease impulsivity via the projections of these neurons to VTA.

D2R-Expressing Neurons in the CeA → BNST Circuit Regulate Impulsive Behavior. We next examined the function of the projections of CeA-D2R neurons to the BNST. Patch-clamp recordings in brain slices prepared from D2R-Cre mice injected with AAV-DIO-ChR2-EYFP revealed that photostimulation of axons of ChR2-expressing CeA-D2R neurons evoked IPSCs in 69% of BNST neurons (31 of 45 neurons). The BNST is primarily populated by GABAergic neurons (33, 34), with the remaining neurons being a heterogeneous mix that includes glutamatergic neurons expressing vesicular glutamate transporters (34, 35). Post hoc immunohistochemical staining of BNST neurons examined electrophysiologically (Fig. 5*A*) revealed that 7 of 10 of the neurons that exhibited synaptic responses to photostimulation of CeA-D2R cells also expressed the VGAT and are thus GABAergic [Fig. 5*B*; $n = 14$ stained cells, $n = 10$ IPSCs (+), $n = 7$ VGAT(+)/IPSC (+)]. The remaining three cells that exhibited light-evoked IPSCs expressed VGlut2 and are glutamatergic. There was no significant difference in the amplitude of light-evoked IPSCs

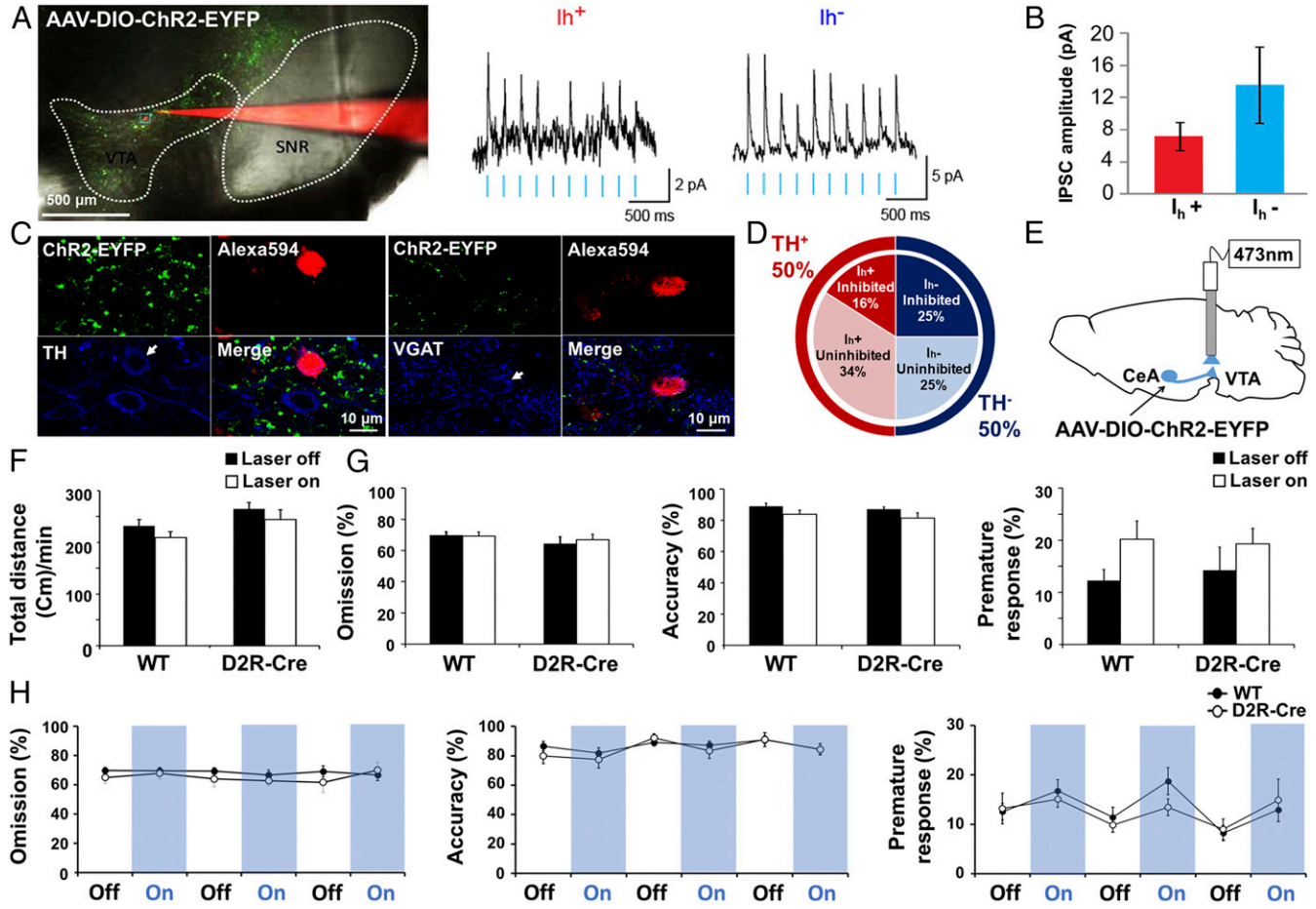

Fig. 4. D2R-expressing neurons in the CeA → VTA circuit did not regulate the impulsive behavior. (*A*) Fluorescence image of a patch-clamped neuron (red) and of ChR2-EYFP–positive axon terminals (green) projecting from the CeA to the VTA [Scale bar, 500 μm (*Left*)] as well as representative recordings of light-evoked IPSCs of I_h^+ and I_h^- neurons in the VTA (*Right*). Traces were low-pass-filtered at a cutoff frequency of 140 Hz. (*B*) Amplitude of photostimulation-evoked IPSCs in I_h^+ ($n = 9$) and I_h^- ($n = 20$) VTA neurons (holding potential, −50 mV). Data were analyzed from eight mice. (*C*) Confocal images of patch-clamped neurons (arrows; labeled red with Alexa Fluor 594) in the VTA of D2R-Cre mice (TH; $n = 8$, VGAT; $n = 10$) injected with AAV-DIO-ChR2-EYFP into the CeA. The neurons were stained with antibodies to TH or to VGAT (blue). (Scale bars, 10 μm.) (*D*) Proportions of VTA neurons examined ($n = 83$) that were positive or negative for photostimulation-induced IPSPs, the I_h current, or TH immunoreactivity ($n = 24$). Data were analyzed from eight mice. (*E*) Schematic diagram of AAV-DIO-ChR2-EYFP injection into the CeA and implantation of a fiber-optic cannula into the VTA of D2R-Cre mice (D2R-Cre$^{CeA\rightarrow VTA}$) for experiments shown in *F*–*H*. (*F*) Total travel distance per minute in the open-field test for WT ($n = 9$) and D2R-Cre$^{CeA\rightarrow VTA}$ ($n = 5$) mice during laser-off and laser-on (3 min, 5 Hz, 10 mW) periods determined as in Fig. 2*F*. $P > 0.05$, genotype × light stimulation interaction; $F_{(1, 24)} = 0.00$ with two-way ANOVA followed by Bonferroni test. (*G*) Percentage omission, accuracy, and premature response in the 5-CSRTT for WT ($n = 13$) and D2R-Cre$^{CeA\rightarrow VTA}$ ($n = 7$) mice as determined in Fig. 2*H*. $P > 0.05$, genotype × light stimulation interaction; $F_{(1, 36)} = 0.18$ with two-way ANOVA followed by Bonferroni test. (*H*) Time course omission (%), accuracy (%), and premature response (%) in the 5-CSRTT as in *G*. All values in the data represent mean ± SEM.

recorded from VGAT-positive and VGAT-negative neurons (Fig. 5 *C* and *D*; $P > 0.1$, Wilcoxon signed-rank test). These results indicate that the majority of BNST neurons, both excitatory and inhibitory, receive inhibitory input from the CeA.

We next examined the behavioral function of CeA-D2R projections to the BNST by photostimulating them in vivo (Fig. 5*E*). CeA-D2R neurons project mainly to ventrolateral (BSTLV), ventromedial (BSTMV), and lateral posterior (BSTLP) parts of the BNST (*SI Appendix*, Fig. S11*A*), so that our optical fibers implanted in the dorsal part of the BNST would be expected to stimulate projections to both the dorsal and ventral parts of the BNST (*SI Appendix*, Fig. S11*B*). Such photostimulation decreased impulsivity, as shown by a significant decrease in the proportion of premature responses in the 5-CSRTT (Fig. 5 *G* and *H*; $n = 8$–17, $F_{(1, 30)} = 7.96$, $P = 0.0084$, and Movies S4 and S5). In contrast, photostimulation of CeA inputs to BNST had no effect on the rate of omissions or accuracy measured in this test (Fig. 5 *G* and *H*), as well as no effect on locomotor activity (Fig. 5*F*) or anxiety-like behavior (*SI Appendix*, Fig. S11*C*). We therefore conclude that D2R-positive neurons in the CeA control impulsive behavior via their projections to the BNST. Furthermore, GABAergic neurons in the BNST that receive inhibitory input from CeA-D2R neurons are the primary mediators of this regulation.

BNST Projection-Specific Recovery of D2R Expression in the CeA of *Drd2*$^{-/-}$ Mice Normalized Impulsivity. To further demonstrate that D2R-expressing CeA neurons projecting to BNST are critical for regulation of impulsivity, we performed a specific rescue of D2Rs in the CeA → BNST circuit via injection of a retrogradely transported virus, AAV2-retro-Ef1a-mCherry-IRES-Cre, into the BNST and of another virus, AAV-DIO-D2R-GFP, into the CeA of *Drd2*$^{-/-}$ mice (Fig. 6*A*). WT and *Drd2*$^{-/-}$ mice injected with AAV-DIO-EYFP were used as controls (Fig. 6*C*). We observed that this strategy resulted in the colocalized expression of GFP (D2R-GFP) and mCherry (Cre-recombinase) in the CeA, indicating a selective restoration of D2R expression in neurons

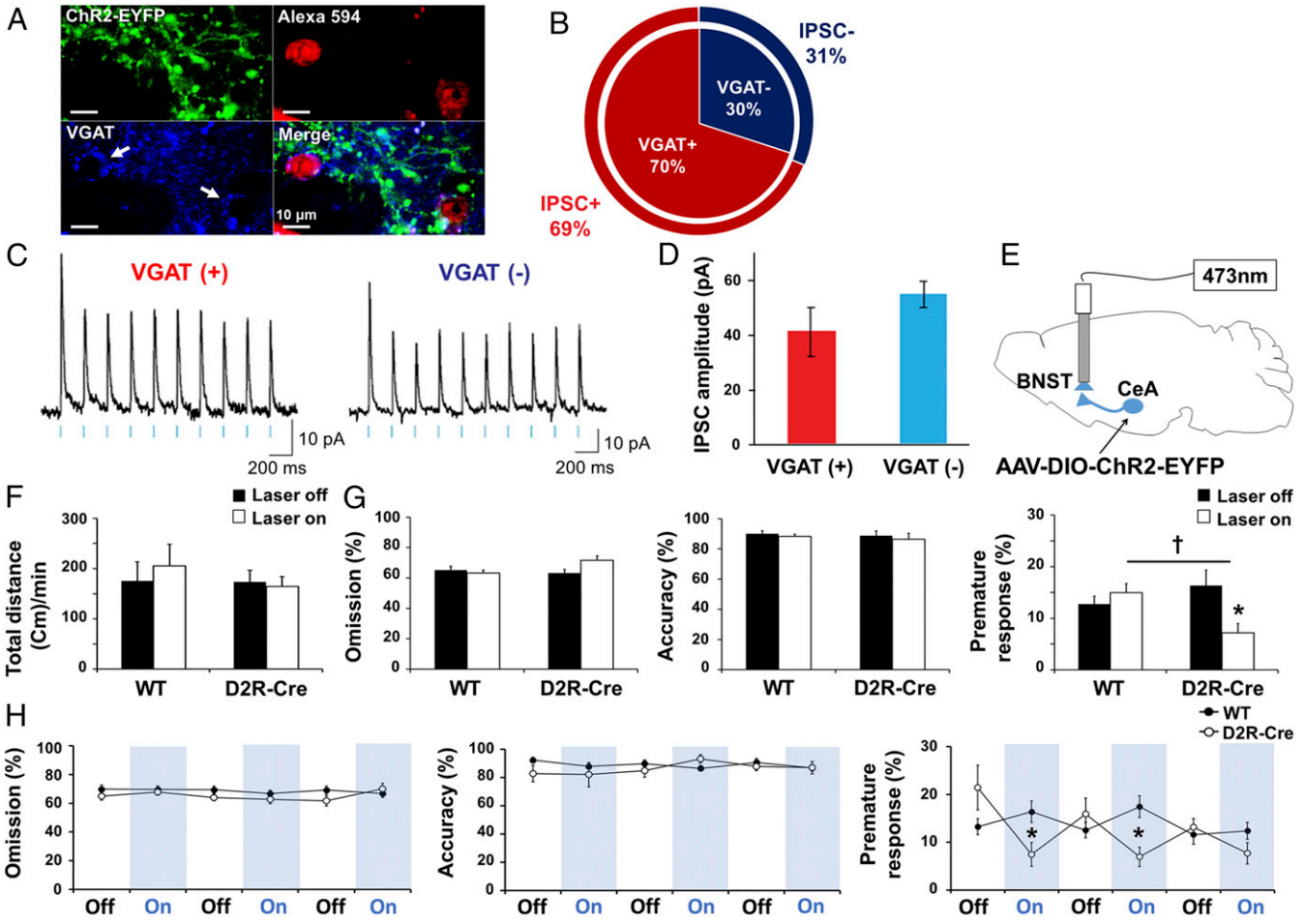

Fig. 5. D2R-expressing neurons in the CeA → BNST circuit regulate impulsive behavior. (*A*) Confocal images of patch-clamped neurons (arrows; labeled red with Alexa Fluor 594) in the BNST of D2R-Cre mice ($n = 2$) injected with AAV-DIO-ChR2-EYFP into their CeA. The neurons were stained with antibodies to VGAT (blue). (*B*) Fraction of BNST neurons examined ($n = 45$) that were positive or negative for photostimulation-induced IPSPs or VGAT immunoreactivity ($n = 14$). Recordings were performed in lateral posterior (BSTLP) and ventral parts of bed nucleus of the stria terminalis (BSTLV) subregions that receive input from D2R-expressing CeA neurons. Percentage of VGAT immunoreactive cells was analyzed as in *A*, and data were obtained from two mice. (*C*) Representative light-evoked IPSCs recorded from VGAT(+) and VGAT(−) neurons in the BNST. IPSC traces are the averages of five trials, measured at a holding potential of −50 mV, and were low-pass-filtered (200 Hz). (*D*) Amplitude of photostimulation-evoked IPSCs in VGAT(+) ($n = 7$) and VGAT(−) ($n = 3$) BNST neurons (holding potential, −50 mV). Data were analyzed from two mice. (*E*) Schematic diagram of AAV-DIO-ChR2-EYFP injection into the CeA and implantation of a fiber-optic cannula into the BNST of D2R-Cre mice (D2R-Cre$^{CeA\rightarrow BNST}$) for analysis in *F*–*H*. (*F*) Total travel distance per minute in the open-field test for WT ($n = 5$) and D2R-Cre$^{CeA\rightarrow BNST}$ ($n = 3$) mice during laser-off and laser-on (3 min, 5 Hz, 10 mW) periods determined as in Fig. 2*F*. $P > 0.05$, genotype × light stimulation interaction; $F_{(1, 12)} = 0.24$ with two-way ANOVA followed by Bonferroni test. (*G*) Percentage omission, accuracy, and premature response in the 5-CSRTT for WT ($n = 17$) and D2R-Cre$^{CeA\rightarrow BNST}$ ($n = 8$) mice as determined in Fig. 2*H*. All values represent mean ± SEM; $*P < 0.05$ versus corresponding laser-off value; $\dagger P < 0.05$ versus corresponding WT; genotype × light stimulation interaction in premature response (%): $F_{(1, 30)} = 7.96$, $P = 0.0084$ with two-way ANOVA followed by Bonferroni test. (*H*) Time course omission (%), accuracy (%), and premature response (%) in the 5-CSRTT as in *G*. $*P < 0.05$ versus the corresponding value for WT (unpaired Student's *t* test). All data are means ± SEM.

that project to the BNST (Fig. 6*B*) although it should be noted that D2R expression in these experiments is not limited to neurons that normally express D2R. We also performed a FISH analysis with a *Drd2*-specific probe, which revealed specific D2R FISH signals after rescuing of D2R expression in the CeA of CeA → BNST projection neurons (Fig. 6*C*). Mice with such projection-specific recovery of D2R were subjected to 5-CSRTT to measure their impulsivity and attention (Fig. 6*D*). This CeA → BNST projection-specific rescue of D2R in *Drd2*$^{-/-}$ mice resulted in a significant normalization of premature responses without an effect on other parameters assessed in the 5-CSRTT (Fig. 6*E*; $\dagger P < 0.05$, $n = 4$). This demonstrates that D2R-expressing CeA neurons that project to the BNST are critical for control of impulsivity.

Discussion

Dysfunctional dopaminergic neurotransmission, especially involving D2R, has been proposed to be a mechanism underlying impulsivity. Evidence for this proposal comes from pharmacological and behavioral analyses in animals, as well as from human brain imaging (5, 9, 13, 14). In the present study, we demonstrated that the absence of D2Rs increases impulsivity. Furthermore, we found that manipulation of D2R expression and optogenetic stimulation of D2R-positive neurons in the CeA modulates impulsive behaviors in mice. These results provide strong evidence that dopaminergic signaling in the CeA is a central neural locus that controls impulsive behaviors through D2R-positive neurons projecting from the CeA to the BNST.

Dopaminergic afferents from the VTA innervate the amygdala, in particular the intercalated paracapsular islands and basolateral amygdala, where D1Rs are mainly distributed, as well as the CeA, where D2Rs are mainly expressed. Although the CeA is well known for its role in fear conditioning, increasing evidence indicates that the CeA also can control other cognitive- and reward-related processes (18, 21, 24). D2R-expressing CeA

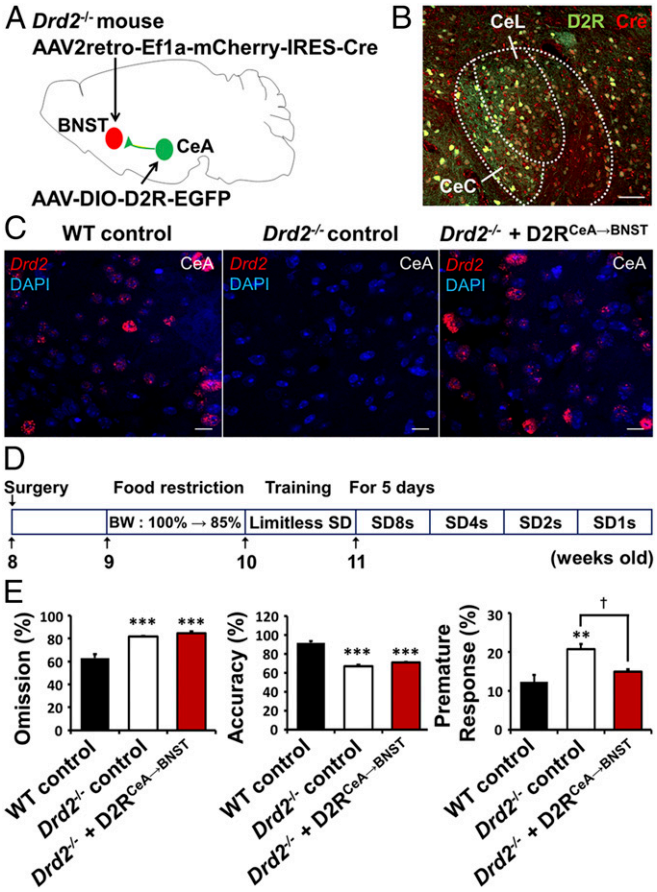

Fig. 6. Projection-specific D2R expression in the CeA → BNST modulates impulsivity. (*A*) Schematic for injection of AAV2-retro-Ef1a-mCherry-IRES-Cre into BNST and AAV-DIO-D2R-EGFP into the CeA of *Drd2*$^{-/-}$ mice for rescue of D2R in *Drd2*$^{-/-}$ mice. (*B*) Injection site shown in a brain section stained with DAPI (blue), EGFP fluorescence (green), and mCherry (red) in the CeA of a *Drd2*$^{-/-}$ mouse ($n = 4$) injected with AAV-Ef1a-mCherry-IRES-Cre and AAV-DIO-D2R-EGFP. CeL, lateral nucleus of the CeA; CeC, the capsular nucleus of the CeA. (Scale bar, 50 μm.) (*C*) Representative histology of CeA with *Drd2* FISH of WT control, *Drd2*$^{-/-}$ control, and D2R$^{CeA→BNST}$ rescued *Drd2*$^{-/-}$ mice. WT and *Drd2*$^{-/-}$ mice injected with AAV-DIO-EYFP were used as controls. (Scale bars, 20 μm.) (*D*) Experimental scheme of the 5-CSRTT. BW, body weight; SD, stimulus duration. (*E*) Percentage of omission, accuracy, and premature response, respectively, in the 5-CSRTT for WT mice injected with AAV-DIO-EYFP (WT control, $n = 4$) or *Drd2*$^{-/-}$ mice injected with AAV-DIO-EYFP (*Drd2*$^{-/-}$ control, $n = 4$) or AAV-DIO-D2R-EGFP (*Drd2*$^{-/-}$ + D2R$^{CeA→BNST}$, $n = 4$). All values represent mean ± SEM; $^{**}P < 0.01$, $^{***}P < 0.001$ versus WT control; †$P < 0.05$ versus *Drd2*$^{-/-}$ control with one-way ANOVA followed by Bonferroni test.

neurons project to the midbrain, including the VTA and the substantia nigra (SN), but also to the BNST. Selective expression of D2R in the CeA may have an important impact on the final behavioral outcome for cognitive- and reward-related processes.

D2R-expressing neurons were predominantly found in the lateral nucleus of the CeA (CeL) and the capsular nucleus of the CeA (CeC) (24, 36). Further analysis revealed that these D2R neurons significantly overlap with a subpopulation of PKCδ-expressing neurons (*SI Appendix*, Fig. S3). Overall, these data are consistent with a recent report (24): some differences in degree of colocalization may be due to differences in techniques and mouse lines used. It has been suggested that CeA PKCδ-expressing neurons inhibit feeding behavior (30) and that a subpopulation of PKCδ-expressing neurons are required for defensive behavior (24, 37). Our finding that D2R neurons significantly overlap with PKCδ-expressing neurons suggests a potential shared connection for behaviors mediated by D2R neurons within the CeA. Future studies will be required to determine how D2R-expressing neurons are connected within the microcircuitry of the CeA and to their input/outputs and how these circuits control impulsive behavior.

The importance of D2R in control of impulsive behaviors has been suggested by previous pharmacological manipulations; for example, systemic injection of D2R agonists decreases impulsivity (13, 14, 38). A role for D2Rs within the NAc in the control of impulsivity has been proposed based on previous studies using local injection of DA agonists and antagonists within the NAc (39), although this conclusion is limited by the significant effect of such injections on attention (40, 41). The 5-CSRTT measurements of behavior have indicated no specific effect on impulsivity in response to injection of D2R agonists and antagonists into the CeA (42). Our study uses specific manipulations of D2R neurons and their related circuits to investigate the role of D2R in the control of impulsivity. Our results demonstrate that impulsivity is selectively affected by knockdown or recovery of D2R within the CeA. Further support comes from our cell-type and pathway-specific optogenetic manipulation of D2R-expressing neurons/circuits in the CeA, which yielded selective changes in impulsivity.

Although optogenetic activation of D2R neurons in the NAc also decreased the premature responses of animals during 5-CSRTT testing, this was accompanied by significant increases in response omission. Therefore, it appears that D2R neurons in the NAc regulate both impulsive behavior and attentional performance. Behavioral changes caused by activation of D2R neurons in the NAc were rather incoherent, showing less impulsivity in conjunction with a deficiency in attention. It remains to be determined whether this is due to heterogeneity of neurons within NAc-associated circuits or is the result of a general cognitive deficit. Recently, it has been reported that chemogenetic activation of DA neurons in either the VTA or substantia nigra pars compacta (SNc) does not affect impulsivity measured in the 5-CSRTT, but instead induces deficits in attentional performance (43). Therefore, while DA release certainly is an important signal to promote reward-related behaviors, the activation of specific DA receptors in a specific circuit will determine the final behavioral output. In this context, our findings, together with other reports (40, 41, 43), reinforce the role of D2Rs within the NAc as an important mediator of attentional performance in the execution of stimulus-induced responses.

We demonstrated that, while D2R-mediated signaling in the CeA influences both the VTA and BNST, D2R-expressing neurons of the CeA → BNST pathway control impulsive behavior. GABAergic neurons of the VTA have previously been shown to inhibit DA neurons (44, 45). Our finding that D2R-expressing neurons in the CeA inhibit both dopaminergic and GABAergic neurons in the VTA indicates that heterogeneity and inhibition–disinhibition balance within CeA → VTA projections will determine the output of the CeA → VTA pathway, which could then gate the control of reward-driven behavior through the mesolimbic DA system (*SI Appendix*, Fig. S12)

The BNST is a component of the extended amygdala, and increasing evidence indicates that the BNST plays a crucial role in diverse physiological functions that include fear formation, anxiety, and feeding behavior, as well as other goal-directed behaviors (46–51). In particular, CeA projections to the BNST appear to mediate interaction among the stress, anxiety, and reward systems (52, 53). A recent study revealed that photostimulation of distinct BNST subregions exerts opposite effects in modulating anxiety, due to the different projections produced by the different neuronal populations of these different subregions (54, 55). In our study, optogenetic manipulation of D2R neurons in the CeA did not affect anxiety behavior, indicating the complexity of circuit dynamics required to form specific behavioral states.

We found that CeA D2R-expressing neurons project to the oval and dorsal parts of the BNST, as well as to the ventral

BNST, and synapse predominantly on GABAergic neurons within the BNST. These D2R-expressing neurons from the CeA are GABAergic, so that optogenetic activation of them inhibits their postsynaptic targets in the BNST. We found that activation of this CeA → BNST inhibitory circuit suppresses impulsive behavior. Furthermore, circuit-specific re-expression indicated that D2Rs in the CeA → BNST projection neurons are critical for suppression of impulsivity. It is not yet clear how expression of D2R, which is thought to be an inhibitory receptor, yields the same behavioral effects as optogenetic stimulation of these neurons. A likely possibility is that D2Rs excite the CeA neurons. Although D2Rs classically are known to couple to Gi/o proteins and to inhibit the excitability of neurons via G-protein–coupled inward-rectifying K^+ channels (56–58), increasing evidence indicates that D2R activation can be excitatory in some cases. For example, Cazorla et al. (59) have shown that chronic up-regulation of D2 receptors increases the excitability of striatal medium spiny neurons via down-regulation of inward-rectifying potassium (Kir2) channels. It has also been shown that D2R can increase the excitability of hilar mossy cells in the hippocampus, an effect that depends on Gi/o and on the Akt/GSK pathway (60). In the lateral amygdala, activation of D2R suppresses feed-forward inhibition and enables the induction of long-term potentiation at excitatory synapses (61). Recently, it has also been reported that D2Rs enhance the excitability of pyramidal neurons in the prefrontal cortex through recruitment of signaling pathways associated with G_s, rather than through conventional Gi/o-associated mechanisms (62). These findings therefore indicate the presence of noncanonical signaling pathways that allow D2Rs to increase neuronal excitability. Further investigation will be required to elucidate how CeA-BNST circuitry regulates impulsive behavior. Such understanding should serve as the basis for therapeutic strategies targeted to neuropsychiatric disorders that are associated with impulsivity.

Methods

Mice. Experiments were performed with male *Drd2*$^{-/-}$ mice (Jackson Laboratory), D2R-Cre Bacterial Artificial Chromosome (BAC) transgenic mice [B6.FVB(Cg)–Tg(Drd2-cre) ER44Gsat/Mmucd; Mutant Mouse Regional Resource Centers], and D2R-EGFP BAC transgenic mice (Mutant Mouse Regional Resource Centers). Mice used for behavioral tests, immunohistochemistry, and electrophysiology were 7- to 8-wk-old *Drd2*$^{-/-}$ mice and 10- to 12-wk-old D2R-Cre and D2R-EGFP mice. Mice were maintained in a specific pathogen-free barrier facility under constant conditions of temperature and humidity and on a 12/12 h light/dark schedule with two to five mice per cage. Animal care and all experimental procedures were performed in accordance with guidelines of the Institutional Animal Care and Use Committees of Korea University and Korea Institute of Science and Technology.

Virus Preparation. The design and preparation of lentivirus-based shRNA-targeting mouse *Drd2* mRNA has been described previously (28). Briefly, the vector pAAV-CMV-D2R-IRES-GFP (pAAV-D2R) was generated by cloning of *Drd2* cDNA into pAAV-CMV-IRES-GFP vector, while pAAV-CMV-GFP (pAAV-GFP) was used as a control. The pAAV-EF1a-DIO-hChR2(H134R)-EYFP-WPRE vector (pAAV-DIO-ChR2-EYFP) was kindly provided by K. Deisseroth, Stanford University, Stanford, California, with corresponding virus particles being produced and concentrated as described above for AAV-D2R. See the *SI Appendix, SI Methods*, for a full description of the protocols used for virus preparation and delivery.

Behavioral Tests. One week after recovery from virus injection and optic-fiber cannula implantation, the basal body weight and food intake of mice were measured, and the mice were then subjected to a food-restriction regimen until reaching 85% of their free-feeding weight. During the 5-CSRTT test (see *SI Appendix, SI Methods*, for more details), each mouse was trained over ∼40 d with a single 30-min session per day. The mouse was first trained to collect food pellets without any response requirement and then to poke its nose into one of the five apertures to obtain food. During the subsequent 5-CSRTT sessions, each trial started with the illumination of the stimulus light in one of the apertures (in pseudorandom order) for a restricted stimulus duration (SD) or until a response was made. Animals had to respond during the presentation of the light stimulus or within a limited hold of 5 s after the termination of the stimulus. Each 5-CSRTT session terminated after a maximum of either 100 trials or 30 min. Nose-poking into the illuminated hole was considered a correct response (the number of correct responses were counted as the number of rewards earned) and was followed by the delivery of a food pellet and the start of a 10-s intertrial interval (ITI), during which the stimulus light was turned off. A nose-poke into a nonilluminated aperture was considered as an incorrect response; the stimulus light was extinguished, and this did not result in the delivery of a food pellet. If an animal did not respond in any of the holes during stimulus presentation or the limited hold, an omission was counted. Nose-poking into the hole before the presentation of the stimulus cue was measured as a premature response. Incorrect responses, omissions, and responses during the ITI resulted in the application of a timeout period of 5 s, during which the house light was turned off. The SD was set at 30 s in the first task session and was decreased in subsequent sessions to 16, 8, 4, 2, and 1 s.

More details regarding optogenetic analysis of the 5-CSRTT and in vivo photostimulation can be found in the *SI Appendix, SI Methods*. The elevated-plus maze and open-field tests were conducted as also described in the *SI Appendix, SI Methods*.

Whole-Field Photostimulation in Brain Slices. In parallel with the patch-clamp recording, photostimuli were applied with the use of a 25× water-immersion objective lens (numerical aperture, 1.05), with the entire width of the microscope field (diameter of ∼500 μm) being illuminated. A mercury arc lamp (USH-1030L; Olympus) was used to provide light, which was then passed through a bandpass filter to activate ChR2 (465–495 nm, 5 mW/mm^2, 10-ms duration at 5 Hz for 2 s) under the control of an electronic shutter (Uniblitz VS25; Vincent).

Statistical Analysis. Differences between two groups were analyzed with the unpaired Student's *t* test, and those among multiple groups were evaluated with one-way or two-way ANOVA followed by appropriate post hoc comparisons. A P value < 0.05 was considered as statistically significant.

Other Methods. Additional experimental procedures are provided in *SI Appendix, SI Methods*.

ACKNOWLEDGMENTS. We thank the staff of the Gyerim Experimental Animal Resource Center for animal care and technical assistance; Joon-Hyun Paik (Duke University) for technical assistance; Dr. Akihiro Yamanaka (Department of Neuroscience II, Research Institute of Environmental Medicine, Nagoya University, Japan) for help with the optogenetic behavioral analysis; and Byeong Jun Kang and Dr. Bok Soon Go (Korea University) for help and discussion. The construct pAAV-EF1a-DIO-hChR2(H134R)-EYFP-WPRE was generously provided by Dr. Karl Deisseroth (Stanford University). This work was supported by Brain Research Program Grant 2013M3C7A1056101; Bio & Medical Technology Development Program Grants 2013M3A9D5072550 and 2016M3A9D5A01952412; Mid-Career Researcher Program Grants 2014R1A2A2A01003337 and NRF-2017R1A2B4008875; Science Research Center Grant 2015R1A5A1009024; a Korea University (KU) Future Research Grant (to J.-H.B.); World Class Institute Program Grant WCI 2009-003 of the National Research Foundation of Korea funded by the Ministry of Science, Information and Communication Technology, and Future Planning of the Republic of Korea; and Singapore Ministry of Education Grant MOE2015-T2-2-095.

1. Dalley JW, Everitt BJ, Robbins TW (2011) Impulsivity, compulsivity, and top-down cognitive control. *Neuron* 69:680–694.
2. de Wit H (2009) Impulsivity as a determinant and consequence of drug use: A review of underlying processes. *Addict Biol* 14:22–31.
3. Dalley JW, Mar AC, Economidou D, Robbins TW (2008) Neurobehavioral mechanisms of impulsivity: Fronto-striatal systems and functional neurochemistry. *Pharmacol Biochem Behav* 90:250–260.
4. Belin D, Mar AC, Dalley JW, Robbins TW, Everitt BJ (2008) High impulsivity predicts the switch to compulsive cocaine-taking. *Science* 320:1352–1355.
5. Dalley JW, et al. (2007) Nucleus accumbens D2/3 receptors predict trait impulsivity and cocaine reinforcement. *Science* 315:1267–1270.
6. Pattij T, Vanderschuren LJMJ (2008) The neuropharmacology of impulsive behaviour. *Trends Pharmacol Sci* 29:192–199.
7. Trifilieff P, Martinez D (2014) Imaging addiction: D2 receptors and dopamine signaling in the striatum as biomarkers for impulsivity. *Neuropharmacology* 76:498–509.
8. Lee B, et al. (2009) Striatal dopamine d2/d3 receptor availability is reduced in methamphetamine dependence and is linked to impulsivity. *J Neurosci* 29:14734–14740.
9. Buckholtz JW, et al. (2010) Dopaminergic network differences in human impulsivity. *Science* 329:532.
10. Limosin F, et al. (2003) Impulsiveness as the intermediate link between the dopamine receptor D2 gene and alcohol dependence. *Psychiatr Genet* 13:127–129.
11. Esposito-Smythers C, Spirito A, Rizzo C, McGeary JE, Knopik VS (2009) Associations of the DRD2 TaqIA polymorphism with impulsivity and substance use: Preliminary results from a clinical sample of adolescents. *Pharmacol Biochem Behav* 93:306–312.

12. Chan TWS, et al. (2014) Impulsivity and genetic variants in DRD2 and ANKK1 moderate longitudinal associations between sleep problems and overweight from ages 5 to 11. *Int J Obes* 38:404–410.
13. Wade TR, de Wit H, Richards JB (2000) Effects of dopaminergic drugs on delayed reward as a measure of impulsive behavior in rats. *Psychopharmacology (Berl)* 150:90–101.
14. Fernando ABP, et al. (2012) Modulation of high impulsivity and attentional performance in rats by selective direct and indirect dopaminergic and noradrenergic receptor agonists. *Psychopharmacology (Berl)* 219:341–352.
15. Bechara A (2005) Decision making, impulse control and loss of willpower to resist drugs: A neurocognitive perspective. *Nat Neurosci* 8:1458–1463.
16. Xie C, et al. (2011) Identification of hyperactive intrinsic amygdala network connectivity associated with impulsivity in abstinent heroin addicts. *Behav Brain Res* 216: 639–646.
17. Ko CH, et al. (2015) Altered gray matter density and disrupted functional connectivity of the amygdala in adults with internet gaming disorder. *Prog Neuropsychopharmacol Biol Psychiatry* 57:185–192.
18. Everitt BJ, Cardinal RN, Hall J, Parkinson JA, Robbins TW (2000) The amygdala: A functional analysis. *Differential Involvement of Amygdala Subsystems in Appetitive Conditioning and Drug Addiction*, ed Aggleton JP (Oxford Univ Press, New York), pp 1–45.
19. Lu L, et al. (2005) Central amygdala ERK signaling pathway is critical to incubation of cocaine craving. *Nat Neurosci* 8:212–219.
20. LeDoux J (2007) The amygdala. *Curr Biol* 17:R868–R874.
21. Janak PH, Tye KM (2015) From circuits to behaviour in the amygdala. *Nature* 517: 284–292.
22. Thiel KJ, et al. (2010) Stimulation of dopamine D2/D3 but not D1 receptors in the central amygdala decreases cocaine-seeking behavior. *Behav Brain Res* 214:386–394.
23. Phillips AG, Ahn S, Howland JG (2003) Amygdalar control of the mesocorticolimbic dopamine system: Parallel pathways to motivated behavior. *Neurosci Biobehav Rev* 27:543–554.
24. Kim J, Zhang X, Muralidhar S, LeBlanc SA, Tonegawa S (2017) Basolateral to central amygdala neural circuits for appetitive behaviors. *Neuron* 93:1464–1479.e5.
25. Sanchez-Roige S, Peña-Oliver Y, Stephens DN (2012) Measuring impulsivity in mice: The five-choice serial reaction time task. *Psychopharmacology (Berl)* 219:253–270.
26. Velázquez-Sánchez C, et al. (2014) High trait impulsivity predicts food addiction-like behavior in the rat. *Neuropsychopharmacology* 39:2463–2472.
27. Cottone P, et al. (2012) Antagonism of sigma-1 receptors blocks compulsive-like eating. *Neuropsychopharmacology* 37:2593–2604.
28. Sim HR, et al. (2013) Role of dopamine D2 receptors in plasticity of stress-induced addictive behaviours. *Nat Commun* 4:1579.
29. Kim J, et al. (2014) Optogenetic mapping of cerebellar inhibitory circuitry reveals spatially biased coordination of interneurons via electrical synapses. *Cell Rep* 7: 1601–1613.
30. Cai H, Haubensak W, Anthony TE, Anderson DJ (2014) Central amygdala PKC-δ(+) neurons mediate the influence of multiple anorexigenic signals. *Nat Neurosci* 17: 1240–1248.
31. Song SS, et al. (2014) Optogenetics reveals a role for accumbal medium spiny neurons expressing dopamine D2 receptors in cocaine-induced behavioral sensitization. *Front Behav Neurosci* 8:336.
32. Margolis EB, Lock H, Hjelmstad GO, Fields HL (2006) The ventral tegmental area revisited: Is there an electrophysiological marker for dopaminergic neurons? *J Physiol* 577:907–924.
33. Kudo T, et al. (2012) Three types of neurochemical projection from the bed nucleus of the stria terminalis to the ventral tegmental area in adult mice. *J Neurosci* 32: 18035–18046.
34. Nguyen AQ, Dela Cruz JAD, Sun Y, Holmes TC, Xu X (2016) Genetic cell targeting uncovers specific neuronal types and distinct subregions in the bed nucleus of the stria terminalis. *J Comp Neurol* 524:2379–2399.
35. Poulin JF, Arbour D, Laforest S, Drolet G (2009) Neuroanatomical characterization of endogenous opioids in the bed nucleus of the stria terminalis. *Prog Neuropsychopharmacol Biol Psychiatry* 33:1356–1365.
36. De Bundel D, et al. (2016) Dopamine D2 receptors gate generalization of conditioned threat responses through mTORC1 signaling in the extended amygdala. *Mol Psychiatry* 21:1545–1553.
37. Han W, et al. (2017) Integrated control of predatory hunting by the central nucleus of the amygdala. *Cell* 168:311–324.e18.
38. van Gaalen MM, van Koten R, Schoffelmeer ANM, Vanderschuren LJMJ (2006) Critical involvement of dopaminergic neurotransmission in impulsive decision making. *Biol Psychiatry* 60:66–73.
39. Moreno M, et al. (2013) Divergent effects of $D_2/_3$ receptor activation in the nucleus accumbens core and shell on impulsivity and locomotor activity in high and low impulsive rats. *Psychopharmacology (Berl)* 228:19–30.
40. Pattij T, Janssen MCW, Vanderschuren LJMJ, Schoffelmeer ANM, van Gaalen MM (2007) Involvement of dopamine D1 and D2 receptors in the nucleus accumbens core and shell in inhibitory response control. *Psychopharmacology (Berl)* 191:587–598.
41. Agnoli L, Mainolfi P, Invernizzi RW, Carli M (2013) Dopamine D1-like and D2-like receptors in the dorsal striatum control different aspects of attentional performance in the five-choice serial reaction time task under a condition of increased activity of corticostriatal inputs. *Neuropsychopharmacology* 38:701–714.
42. Smith ES, Fabian P, Rosenthal A, Kaddour-Djebbar A, Lee HJ (2015) The roles of central amygdala D1 and D2 receptors on attentional performance in a five-choice task. *Behav Neurosci* 129:564–575.
43. Boekhoudt L, et al. (2017) Chemogenetic activation of midbrain dopamine neurons affects attention, but not impulsivity, in the five-choice serial reaction time task in rats. *Neuropsychopharmacology* 42:1315–1325.
44. van Zessen R, Phillips JL, Budygin EA, Stuber GD (2012) Activation of VTA GABA neurons disrupts reward consumption. *Neuron* 73:1184–1194.
45. Tan KR, et al. (2012) GABA neurons of the VTA drive conditioned place aversion. *Neuron* 73:1173–1183.
46. Dong HW, Petrovich GD, Watts AG, Swanson LW (2001) Basic organization of projections from the oval and fusiform nuclei of the bed nuclei of the stria terminalis in adult rat brain. *J Comp Neurol* 436:430–455.
47. Duvarci S, Bauer EP, Paré D (2009) The bed nucleus of the stria terminalis mediates inter-individual variations in anxiety and fear. *J Neurosci* 29:10357–10361.
48. Somerville LH, Whalen PJ, Kelley WM (2010) Human bed nucleus of the stria terminalis indexes hypervigilant threat monitoring. *Biol Psychiatry* 68:416–424.
49. Jennings JH, Rizzi G, Stamatakis AM, Ung RL, Stuber GD (2013) The inhibitory circuit architecture of the lateral hypothalamus orchestrates feeding. *Science* 341: 1517–1521.
50. Jalabert M, Aston-Jones G, Herzog E, Manzoni O, Georges F (2009) Role of the bed nucleus of the stria terminalis in the control of ventral tegmental area dopamine neurons. *Prog Neuropsychopharmacol Biol Psychiatry* 33:1336–1346.
51. Dumont EC, Mark GP, Mader S, Williams JT (2005) Self-administration enhances excitatory synaptic transmission in the bed nucleus of the stria terminalis. *Nat Neurosci* 8:413–414.
52. Oler JA, et al. (2009) Serotonin transporter availability in the amygdala and bed nucleus of the stria terminalis predicts anxious temperament and brain glucose metabolic activity. *J Neurosci* 29:9961–9966.
53. Yassa MA, Hazlett RL, Stark CEL, Hoehn-Saric R (2012) Functional MRI of the amygdala and bed nucleus of the stria terminalis during conditions of uncertainty in generalized anxiety disorder. *J Psychiatr Res* 46:1045–1052.
54. Jennings JH, et al. (2013) Distinct extended amygdala circuits for divergent motivational states. *Nature* 496:224–228.
55. Kim SY, et al. (2013) Diverging neural pathways assemble a behavioural state from separable features in anxiety. *Nature* 496:219–223.
56. Innis RB, Aghajanian GK (1987) Pertussis toxin blocks autoreceptor-mediated inhibition of dopaminergic neurons in rat substantia nigra. *Brain Res* 411:139–143.
57. Lacey MG, Mercuri NB, North RA (1987) Dopamine acts on D2 receptors to increase potassium conductance in neurones of the rat substantia nigra zona compacta. *J Physiol* 392:397–416.
58. Uchida S, Akaike N, Nabekura J (2000) Dopamine activates inward rectifier K+ channel in acutely dissociated rat substantia nigra neurones. *Neuropharmacology* 39: 191–201.
59. Cazorla M, Shegda M, Ramesh B, Harrison NL, Kellendonk C (2012) Striatal D2 receptors regulate dendritic morphology of medium spiny neurons via Kir2 channels. *J Neurosci* 32:2398–2409.
60. Etter G, Krezel W (2014) Dopamine D2 receptor controls hilar mossy cells excitability. *Hippocampus* 24:725–732.
61. Bissière S, Humeau Y, Lüthi A (2003) Dopamine gates LTP induction in lateral amygdala by suppressing feedforward inhibition. *Nat Neurosci* 6:587–592.
62. Robinson SE, Sohal VS (2017) Dopamine D2 receptors modulate pyramidal neurons in mouse medial prefrontal cortex through a stimulatory G-protein pathway. *J Neurosci* 37:10063–10073.